Heliyon 9 (2023) e16738

Contents lists available at ScienceDirect

Heliyon

journal homepage: www.cell.com/heliyon

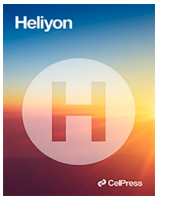

Efficient photodegradation of methyl red dye by kaolin clay supported zinc oxide nanoparticles with their antibacterial and antioxidant activities

Tamanna Gul [a], Idrees Khan [a,*], Bashir Ahmad [b,c], Shujaat Ahmad [d], Ahad Amer Alsaiari [e], Mazen Almehmadi [e], Osama Abdulaziz [e], Abdulaziz Alsharif [e], Ibrahim Khan [f,***], Khalid Saeed [a,**]

[a] Department of Chemistry, Bacha Khan University, Charsadda, KP, Pakistan
[b] Centre of Biotechnology & Microbiology University of Peshawar, Peshawar, KP, Pakistan
[c] Institute of Biotechnology and Microbiology, Bacha Khan University, Charsadda, KP, Pakistan
[d] Department of Pharmacy, Shaheed Benazir Bhutto University, Sheringal, 18050, Pakistan
[e] Department of Clinical Laboratory Sciences, College of Applied Medical Sciences, Taif University, Taif 21944, Saudi Arabia
[f] School of Chemical Engineering and Materials Science, Chung-Ang University, 84 Heukseok-ro, 06974 Seoul, South Korea

ARTICLE INFO

Keywords:
Kaolin clay
Photodegradation
Methyl red
Bioactivity
Antioxidant activity

ABSTRACT

Kaolin clay-supported Zinc oxide (ZnO/KC) and ZnO NPs nanoparticles (NPs) were prepared by a chemical reduction process and used for the photodegradation of methyl red (MR) dye as a photocatalyst. Due to the interlayered porous structure of the KC, we achieved an extremely good association between ZnO NPs and KC. The product confirmation was conducted by Scanning electron microscopy (SEM), X-Ray diffraction (XRD), energy dispersive X-Ray (EDX), and Fourier transforms infrared (FTIR). SEM showed the irregular morphology of ZnO NPs, while ZnO/KC NCs were predominately round-shaped. Moreover, in both cases, NPs were present in both dispersed as well as agglomerated forms with an average particle size below 100 nm. The results acquired from photodegradation analyses show that ZnO NPs and ZnO/KC NCs degraded about 90 and 99% of MR dye respectively, under UV light in a short irradiation time of 10 min. The recovered and re-recovered ZnO NPs and ZnO/KC NCs also considerably photodegraded MR dye in an aqueous medium. The same NPs also exhibit promising bioactivities against two pathogenic bacteria, i.e., *Citrobacter* and *Providencia*. The antioxidant activity of ZnO/KC NCs reached to reasonable 70% compared to the 88% activity of the standard ascorbic acid.

1. Introduction

Organic dyes have been used widely for various industrial colouring processes [1] in different industries like textile, pulp, paper, leather, cosmetics, dyestuffs, food packaging, plastic and chemical industries [2–4]. The industrial syntheses and manufacturing

* Corresponding author.
** Corresponding author.
*** Corresponding author.
E-mail addresses: idreeschem_uom@yahoo.com (I. Khan), ebraheem.chemist@gmail.com (I. Khan), khalidkhalil2002@yahoo.com (K. Saeed).

https://doi.org/10.1016/j.heliyon.2023.e16738
Received 28 February 2023; Received in revised form 24 May 2023; Accepted 25 May 2023
Available online 26 May 2023

processes bring up about ~20% organic dyes loss to aquatic environments [5]. The discharged dyes containing wastewater into the natural environment severely damage the ecosystem and cause a series of hazards to humans upon exposure, like anaemic, carcinogenesis and neurological disorders [6]. These pollutants are highly toxic and carcinogenic and can be harmful to human health as well as to the environment [7]. The carcinogenic and mutagenic effects of dye molecules in wastewater may cause nervous disorders, and abnormal functioning of the reproductive system, kidneys, liver and brain [8]. Various approaches were tried for the removal of dyes from waste water such as adsorption, ozonation, nanofiltration, biodegradation, coagulation and phytoremediation etc [9–14]. These conventional approaches are expensive, difficult, and destructive and transform pollutants into sludge [15].

Photocatalysis is a simple approach to resolve the discharged dye issue and minimise water pollution problems. Through this process, the degradation of a variety of dyes ensued within aquatic media [16–18]. For this purpose, nanomaterials-based photocatalysts have been found more efficient to convert the typical dye molecules to CO_2, H_2O and other harmless by-products [19]. Nano-sized photocatalysts have much-improved degradation aptitudes to speed up chemical reactions upon absorption of light compared to conventional catalytic materials [20]. The semiconductor oxide NPs offered good paradigms for photocatalysis of dye degradation due to their improved optoelectrical efficiencies, chemical stability, high surface area, uniform pore size, and low photo-corrosion [21]. The most regarded NPs photocatalysts included TiO_2 [22], MnO_2 [23], CuO [24], ZnO NPs [25] etc. Among these, ZnO NPs is an n-type semiconductor, with a wide bandgap of 3.37 eV and a high excitation binding energy of 60 mV, generating electron–hole pairs under light irradiation. ZnO NPs exhibited great potential and high efficiency in degrading organic dyes owing to good chemical stability, low cost and high photosensitivity [26]. Due to these characteristics, ZnO NPs are extensively explored as photocatalysts for the photodegradation of antibiotics [27], pesticides [28], dyes [29–31] etc. However, it only absorbed UV light and was vulnerable to photocorrosion (high recombination rate of the photo-induced charges) in suspended forms due to uncontrollable aggregation in bulk solution due to extremely high specific energy [32]. This impacted their photocatalytic performance immensely and made these NPs unsuitable for multiple photocatalytic usages. Furthermore, their separation from solution media is a wide research challenge [33]. Among various dyes, methyl red (MR) is a monoazo textile dye that is highly toxic, carcinogenic, and mutagenic water pollutants if excrete in a larger amount into aqueous fields. It could cause eye and skin irritations and impacts digestive and respiratory tracts if swallowed/inhaled. Moreover, their low biodegradability owing to the presence of benzene rings makes them further lethal [34]. So, its degradation is a foremost research objective in modern industrial research.

We have presented a facile approach to overcome the mentioned shortcomings by depositing ZnO NPs on a stable Kaolin clay support to acquire ZnO/KC nanocomposite (NC). The as-synthesized materials were characterized by various instrumental techniques like SEM, EDX, FTIR and XRD. The choice of selecting ZnO/KC NCs is based on the fact that until now extremely limited approaches have been dedicated to depositing ZnO NPs over the Kaolin clay surface and applying for dye-decontaminating from the wastewater. Kaolin clay is the most common natural inorganic clay, existing in rocks copiously in crystalline structure [35]. Kaolin mainly consists of kaolinite which has the basic chemical structure of aluminum silicate hydrate ($Al_2Si_2O_5(OH)_4$) [36]. Thus clay is chemically and thermally stable, economical and high melting point [37]. Kaolin (name from Kao-ling hill in China) clay is a white colour soft clay, which is mainly used in the production of paint, paper, rubber and many other materials [38]. It is widely used due to its low cost, and brilliant physical and chemical properties like high porosity, interlayered structure, water holding and ion exchange capacity, reactivity and specific surface area [39,40]. The ZnO NPs and ZnO/KC NCs photocatalysts were used for the photocatalytic degradation of chemically robust MR dye in aqueous media under UV-light irradiation. The influence of various affecting parameters such as irradiation time, catalyst dosage, initial dye concentration, pH of the medium and catalyst sustainability were evaluated. Based on obtained outcomes, it can be established that Kaolin-based support can be extensively employed for diverse types of NPs to enhance their photocatalytic efficiency in terms of recyclability and durability.

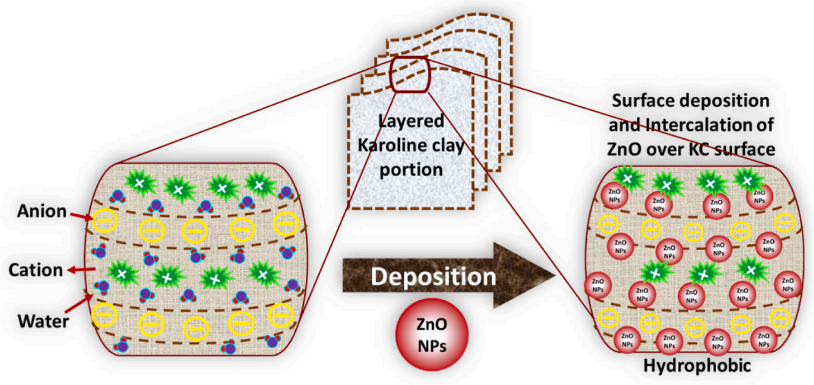

Fig. 1. Schematic of ZnO/KC NCs formation.

2. Experimental work

2.1. Materials and instrumentation

Zinc chloride ($ZnCl_2$) and MR dye were purchased from Sigma Aldrich. The NaOH and HNO_3 were obtained from the Riedel-de Haen chemical company. Kaolin clay was collected from Swat, KP Pakistan.

2.2. Preparation of ZnO/KC NCs

ZnO/KC NCs were prepared through the chemical reduction method. In a simple strategy, 100 mL of Zinc chloride (0.3 M) solution and Kaolin (1 g) were taken in a round bottom flask and stirred until homogenous dispersion. Solution of NaOH (1 M) was added dropwise into it until basic pH was obtained and then refluxed for 2 h at 80 °C with constant stirring. The $ZnCl_2$ gets converted into Zn $(OH)_2$ with the dropwise addition of NaOH which finally converted into ZnO after drying and heating as shown in equations (1) and (2). The synthesized ZnO/KC NCs were then separated via filtration and washed several times with double distilled water to neutralize the pH and to remove any attached chemical/impurities and then dried in an oven at 100 °C. The ZnO NPs were prepared through the same method except using Kaolin. The synthesis schematic representation of the synthesis process can be seen in the following Fig. 1.

$$ZnCl_2 + 2NaOH \longrightarrow Zn(OH)_2 + 2NaCl \quad (1)$$

$$Zn(OH)_2 \longrightarrow ZnO + H_2O \quad (2)$$

2.3. Photodegradation of methyl red dye

From 100 ppm original solution of MR dye, 10 mL dye and 0.02 g of ZnO NPs and ZnO/KC NCs were separately taken in separate beakers and placed in UV light. After specific irradiation time, ZnO NPs and ZnO/KC NCs were separated through centrifugation and degradation of MR was examined via UV–Vis spectrophotometer. The degradation rate (% degradation) of MR was found by equation (3).

$$\text{Degradation rate } (\%) = \left(\frac{A_0 - A}{A_0}\right) \times 100 \quad (3)$$

Where $\mathbf{A_o}$ shows the initial absorbance and **A** shows the dye absorbance after UV irradiation.

2.4. Characterization

The SEM and EDX analyses ZnO NPs and ZnO/KC NCs were conducted by SEM LA-6490, JEOL Japan (energy range of 0–20 keV) and EDX- INCA 200/Oxford Instruments, company oxford, UK, respectively. The FT-IR and XRD analyses were individually performed by FT-IR spectrometer (PerkinElmer, serial number 95120) and XRD Model JEOL-300. The photodegradation study of MR was conducted via UV–Vis spectrophotometer (Model UV-1800, Shimadzu, Japan).

2.5. Antioxidant activity

2,2-diphenyl-1-picrylhydrazyl (DPPH) (a stable radical generating chemical) was used to find the antioxidant activity of the synthesized ZnO NPs and ZnO/KC NCs in terms of free radical scavenging ability. Various doses (100, 200 and 300 μg/mL) of synthesized NPs were dispersed in dimethyl sulfoxide (DMSO). Then 2.5 mL of DPPH (0.1 mM solution as prepared in DMSO) was added to each NPs concentration and was kept for 30 min at 25 °C. The absorbance spectra of all concentrations were recorded and measured at a wavelength maxima of ~500 nm. DMSO (0.1 mM) solution of DPPH was used as a control, while DPPH was used as a reference standard.

The % DPPH scavenging effect was determined by equation (4).

$$\text{DPPH scavenging } (\%) = \left(\frac{Abs\ control - Abs\ test}{Abs\ control}\right) \times 100 \quad (4)$$

2.6. Antibacterial activity

Pathogenic bacteria *Citrobacter* and *Providencia* were collected from the department of pathology, medical and teaching institute, Hayat Abad medical complex, Peshawar (Pakistan). The Agar well diffusion method was used for the determination of the antibacterial activity of synthesized ZnO NPs and ZnO/KC NCs against the pathogens. Agar 8.4 g (media) was dissolved in 300 mL distilled water and then autoclaved for 15 min at 121 °C and cool up to 40 °C. 40–50 mL media was sterile in a Petri dish (14 cm diameter) and then allowed to solidify for the growth of bacteria. 8 mm wells were made by sterile cork borer and the sample code was marked. 10 μL refreshed single colony of bacterial culture was spread equally on the plates of nutrient agar. Different concentration (25, 50, 75 and

100 μL) of the sample was added to respective agar well plate according to bacterial culture. The plates were incubated at 37 °C for 24 h and the zone of inhibition was measured.

3. Results and discussion

3.1. XRD and FTIR analysis

Fig. 2a illustrates XRD patterns of ZnO NPs and ZnO/KC NC. The XRD pattern of ZnO NPs centred at 2θ values of 31.29, 34.84°, 36.2°, and 47.46° confirmed the typical crystal planes of hexagonal ZnO NPs structures. As shown in the orange shaded area in Fig. 2a, the same set of patterns has also appeared in the ZnO/KC NCs spectra, which affirmed the successful deposition of ZnO NPs over the KC surface [38,41,42]. Most of the KC planes are overshadowed by the bulk accumulation of ZnO NPs (37 wt % of Zn in EDX confirm this), however, low-intensity diffraction peaks (denoted as K in XRD spectra of ZnO/KC NCs) at 12°, 26.9° and 44.3° were ascribed to Kaolinite in ZnO/KC NCs. Furthermore, the XRD pattern confirmed that the synthesized ZnO/KC particles were highly crystalline in nature. The particle sizes of the ZnO NPs and ZnO/KC NCs were <20 nm as calculated by the Scherrer equation. Additionally, FTIR spectra of ZnO NPs and ZnO/KC NCs were also supplied in Fig. 2b. As marked in orange specifically, two distinct regions can be visualized in the FTIR spectra of recorded samples. The region below 1000 cm^{-1} is usually ascribed to the stretching frequencies of metal oxides and we believe that in our case these peaks appeared due to the stretching of Zn–O bonds predominantly as reported elsewhere [43]. In the second region from 3000 to 3500 cm^{-1}, the O–H stretching peaks appeared due to moisture adsorption. As expected, the spectrum of ZnO/KC NCs showed a comparatively stronger adsorption band at 3626–3696 cm^{-1} compared to ZnO, which might be due to the –OH vibration as the sample can absorb moisture due to its highly porous nature [44]. The presence of further shoulder bands 1100 cm^{-1} in the spectrum of ZnO/KC NCs might possibly arise from the stretching vibrations of Si–O, Ti–O–Si, and Si–O–Al bonds [42,45]. Moreover, The table in Fig. 2c shows the peak position, full width at half maximum (FWHM), crystalite size (D), and average particle size for main peaks obtained from XRD pattern of ZnO/KC. The Scherrer equation can be used to calculate the crystalite size (D) from the FWHM and peak position using formula $D = K\lambda/(B\cos\theta)$, where K is a constant (usually taken as 0.9), λ is the wavelength of X-ray radiation (0.154 A in this case), B is the FWHM, and θ is the angle of diffraction [46,47]. The calculated average particle size is ~19 nm from Scherrer formula.

3.2. Morphological and structural analyses

The catalytic activity of NPs is greatly affected by the particle size and surface area of NPs. Fig. 3a present that ZnO NPs have pseudo-round irregular shapes distributed in both dispersed and agglomerated forms. It was also found that some of the ZnO NPs are present in the form of large clusters (inset magnified ZnO NPs SEM in Fig. 3a). Fig. 3b shows that the ZnO/KC NCs are very small and have pseudo-round shapes. The size of ZnO/KC NCs was well below 100 nm and aggregated largely. Importantly, the surface of Kaolin clay was almost covered with ZnO NPs. Furthermore, the EDX spectrum of ZnO NPs in Fig. 3a displays corresponding Zinc and Oxygen peaks which confirmed the formation of ZnO NPs. The % atomic and % weight composition values of ZnO NPs were tabulated in the

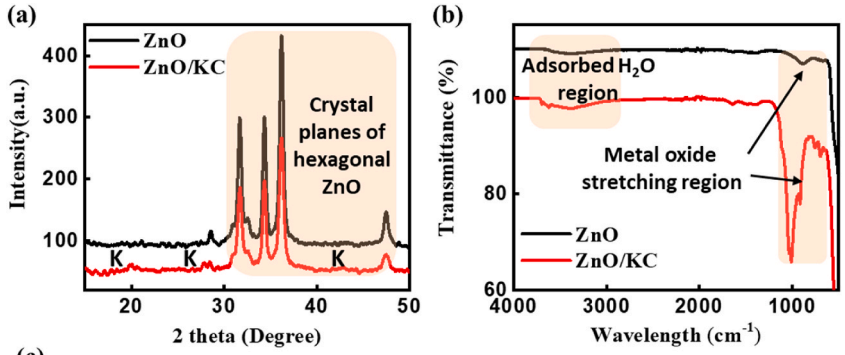

(c)

Peak Position	FWHM	Crystalite size (D)	Average size
67.865	0.501	19.068	19.417
62.797	0.485	19.168	
56.524	0.454	19.829	
36.192	0.439	19.026	
34.352	0.382	21.757	
31.698	0.467	17.652	

Fig. 2. **(a)** XRD patterns and **(b)** FTIR spectra of ZnO NPs and ZnO/KC NC. (c) A table sowing the particle size determintation from the XRD pattern of ZnO/KC.

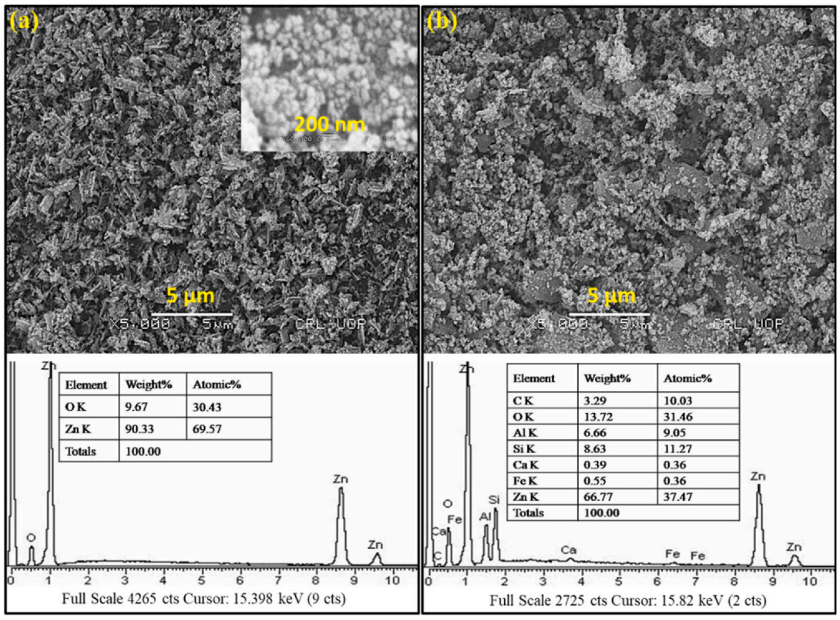

Fig. 3. SEM (top) and EDX (bottom) images of **(a)** ZnO NPs, and **(b)** ZnO/KC NCs.

inset table in the EDX image. Similarly, the EDX spectrum of ZnO/KC NCs in Fig. 3b also presented respective peaks for Zn, O, Si, Al, Ca, Fe, and C elements. The peaks correspondingly appeared from the presence of aluminium, silicon, iron, oxygen, and calcium which are the basic constituents of Kaolin clay, while the Zn peak appeared from the deposited ZnO NPs. The % atomic weight value of Zn in ZnO/KC NCs confirmed the appreciable deposited amount of ZnO NPs over the KC surface.

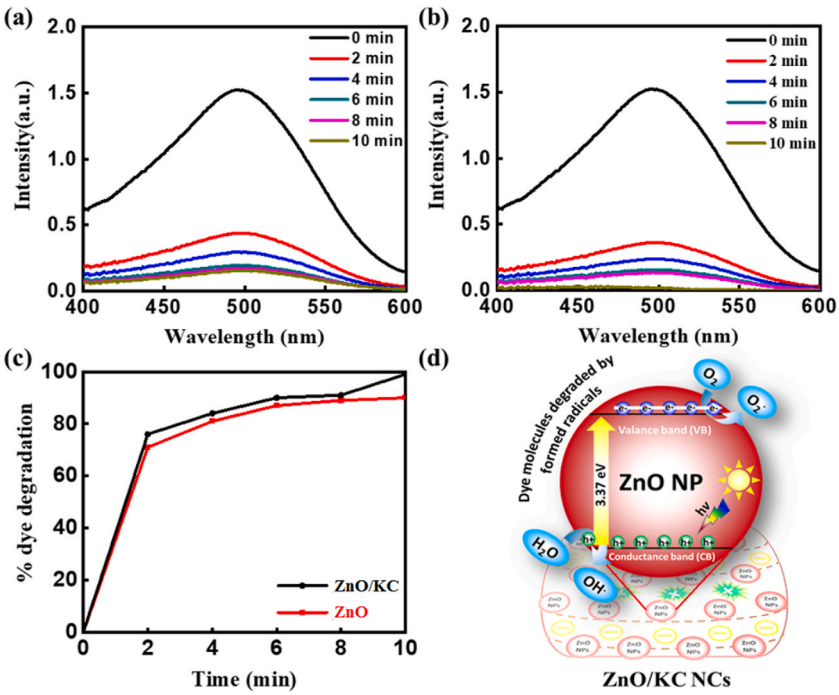

Fig. 4. UV–Vis absorbance spectra obtained from MR degradation by **(a)** ZnO NPs **(b)** ZnO/KC NCs. **(c)** % degradation comparison of both photocatalysts. **(d)** The mechanism of photodegradation of MR by Kaolin-supported ZnO NPs.

3.3. Photodegradation study of methyl red

3.3.1. Irradiation time study

Fig. 4a and b demonstrates the UV/VIS spectra of MR dye, which was photodegraded by ZnO NPs and ZnO/KC NCs under UV-light irradiation. The absorbance maxima in all cases lay at ~500 nm and hence this value is selected to compare the photodegradation efficiency of each sample over regular periods. The results presented that the photodegradation of MR increases with increasing irradiation time. Moreover, the ZnO/KC NCs degrading efficiency is considerably high compared to ZnO NPs. As shown in Fig. 4c, the ZnO NPs and ZnO/KC NCs degraded dye about 90 and 99%, respectively in a very short time of irradiation (10 min) under UV light irradiation. Various ZnO and ZnO based nanomaterials are applied as photocatalysts for MR dye degradation such as seaweed mediated ZnO NPs [19], ZnO nanorods [48], S-scheme ZnO–CoTe binary photocatalyst [49], silica@ZnO nanohybrids [50], ZnO/CdS heterostructures [51], ZnO-GNc [52] etc. These studies shows hard reaction conditions and long irradiation reaction times. As compared to these studies our prepared ZnO/KC NCs degraded 99% dye in 10 min. The high activity of the ZnO/KC NCs is due to the great Kaolin support which facilitated the uniform deposition of ZnO NPs on the surface to enhance their exposure to irradiating light. Moreover, the hydrophilic nature of KC is equally important to allow the dye-containing water to seep inside that trapping improved the reaction time of ZnO with dye molecules and hence boost the overall efficiency of ZnO/KC NCs by almost 9%.

To support our claim, we have provided a scheme of a well-established mechanism of MR in the presence of ZnO NPs and ZnO/KC NCs in Fig. 4d with the literature support [53,54]. As can be seen, the ZnO NPs are shown to be deposited on the KC surface. We have purposely magnified one ZnO NP to show the mechanism. When UV light is passed, excitation of electron (e−) occurs from the valence band (VB) to the conduction band (CB) that generates positive holes (h^+) in the VB, the holes might have reacted with water (H_2O)

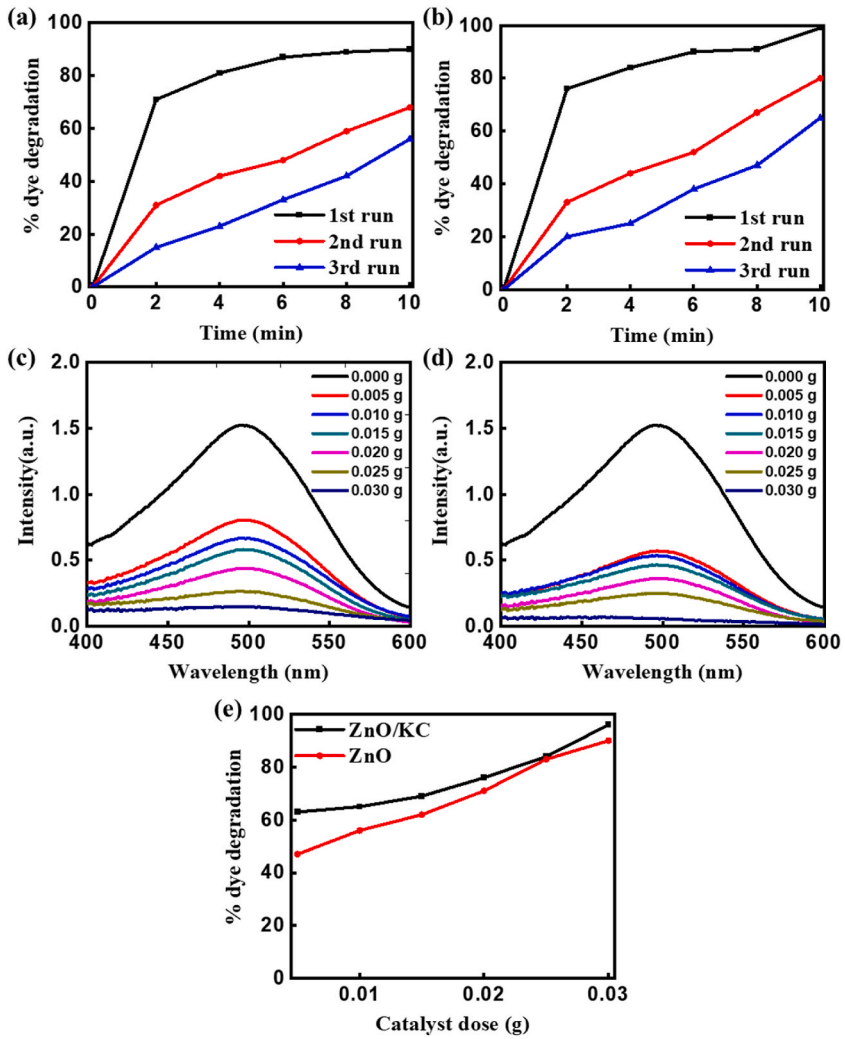

Fig. 5. (a,b) % dye degradation comparison of fresh (1st run), recover (2nd run) and re-recover (3rd run) ZnO NPs and ZnO/KC NCs. **(c,d)** UV–Visible spectra of MR dye photodegraded by different doses of ZnO NPs and ZnO/KC NCs, and **(e)** Comparative dose effect on the % degradation of ZnO NPs and ZnO/KC NCs.

molecules and form hydroxyl radicals (OH•), while the oxygen reacted with the photo-generated electrons and form superoxide anion radical (O_2^-). Both these species (hydroxyl and superoxide anion radical) are highly oxidizing in nature and easily attacked the absorbed organic molecules over ZnO/KC NC or found near the surface of the catalyst that resulted in the degradation of organic molecules (MR in our case) [55,56]. According to the literature using ZnO for the photodegradation of MO dye, $^{\bullet}O_2^-$ serve as the main ROS in the MR degradation, while •OH played a little role [57–59].

3.3.2. Sustainability of photocatalyst and effect of dose

The sustainability of both ZnO NPs and ZnO/KC photocatalysts against MR dye was additionally studied using the same experimental parameters. The used NPs were separated from the dye solution via centrifugation and washed many times with distilled water and then oven dried at 100 °C and used for the second (1st time recovered photocatalysts) and third time (2nd time recovered photocatalysts). Fig. 5 represents the % dye degradation comparison of fresh (1st run), recovered (2nd run) and re-recovered (3rd run) ZnO NPs and ZnO/KC NCs. It is observed that the after 1st run the photocatalytic activity is significantly reduced due to possible agglomerations of ZnO NPs and binding loss between ZnO NPs and KC. It is obvious from Fig. 5a and b that fresh ZnO NPs and ZnO/KC degraded MR dye more effectively than the recovered and re-recover NPs. The fresh ZnO NPs degraded about 90% of the dye while recovered and re-recovered ZnO NPs degraded about 68% and 56%, respectively. Similarly, the fresh ZnO/KC degraded about 99% of dye while the recovered and re-recovered ZnO/KC NCs degraded about 80% and 65% of dye, respectively within 10 min of irradiation time under UV light. Besides the upper mentioned reasons, blockage of the catalyst active site by the photo-insensitive hydroxides deposition is another possible reason that led to the loss of photocatalytic activity [55]. Fig. 5c and d shows the impact of various photocatalyst dose concentrations on the MR dye degraded at constant irradiation time (2min) and dye concentration (100 ppm). The comparative data is provided in Fig. 5e. It can be seen that the dye degradation increased with the photocatalyst dose. In the case of ZnO/KC NCs, 63% of the dye is degraded after 2 min of UV exposure compared to 47% degradation by ZnO NPs at 0.005 g doses. The degradation successfully reached 90% and 96% for 0.030 g concentration of ZnO NPs and ZnO/KC NCs, respectively.

3.3.3. Effect of dye concentration and medium pH

The effect of dye concentration on photodegradation under a constant catalyst amount (0.02 g) and irradiation time of 2 min was investigated and was noted that dye degradation decreased as increased initial dye concentration. Fig. 6a indicates that the rate of dye degradation was inversely affected by the dye concentration. It was realized that at 50 ppm dye concentration, the degradation by ZnO NPs and ZnO/KC NCs effectively reached 80% and 87% dye, respectively. However, as expected the degradation showed gradual retardation with increasing the initial dye concentration. For instance, at 250 ppm in 2 min of irradiation time, the ZnO NPs and ZnO/KC individually remove only 40% and 46% of the MR dye from the aqueous medium. The most probable reason for this behaviour can be related to the fact that with increasing the dye′s initial concentration, the optimum amount got adsorbed on the catalyst surface however a major chunk of dye remained unabsorbed and impacted the light penetration due to the shadowing effect. Thus, least OH· radicals are initiated and we observe comparatively less dye degradation with an initial dye concentration increase [60,61].

Industries discharge their wastewater containing dyes at a different pH, so it is very important to study the pH effect on dye degradation. The pH study was conducted at pH 3, 5, 9 and 11 where dye concentration (100 ppm), catalyst amount (0.02 g) and irradiation time (2 min) was kept constant. The pH of the dye solution was adjusted by adding HNO_3 and NaOH. Fig. 6b reveals the influence of pH on the photodegradation of MR, which illustrated that the degradation of dye increased as decreased in pH of the solution occur i.e., maximum degradation occurred in an acidic medium and about 53% and 57% of the dye was degraded by ZnO NPs and ZnO/KC NCs at pH 11, which was gradually increased to 90% and 95%, respectively at a pH value of 3. The results also declared that ZnO/KC NCs are more active than ZnO NPs. The high degradation at low pH is attributed to the strong Lewis base behaviour of designed catalysts and enhanced adsorption of the dye on the positively charged catalyst surface as reported elsewhere [62].

3.4. Antibacterial activity of ZnO NPs and ZnO/KC NCs

Metal nanoparticles have amazing properties like concentration, chemical composition, shape, size and photoactivation, which

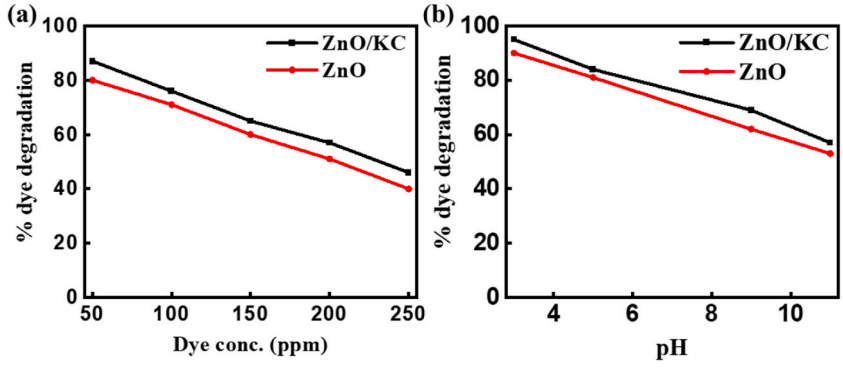

Fig. 6. Comparison of dye degradation by ZnO NPs and ZnO/KC NCs at **(a)** different initial MR dye concentrations and **(b)** various pH values.

make them efficient for antimicrobial properties [63]. ZnO NPs and ZnO/KC NCs were also used for the antibacterial activity against two pathogenic bacteria (*Citrobacter* and *Providencia*). The zone of inhibition was determined in millimetres (mm). Fig. 7a and b represents the digital photographs of antibacterial activities of ZnO NPs against *Citrobacter* and *Provedincia* respectively, while Fig. 7c represents their graphical comparison. Similarly 7d and 7e represents the digital photographs of antibacterial activities of ZnO/KC NCs against *Citrobacter* and *Provedincia* respectively, while Fig. 7f represents their graphical comparison. As comprehensively demonstrated in Fig. 7, ZnO NPs and ZnO/KC NCs significant activity against pathogenic bacteria. 21 and 24 mm of inhibition zone was found against *Citrobacter* and 22 and 23 mm of inhibition zone was found against *Providencia* by ZnO NPs and ZnO/KC NCs, respectively at 100 μL of concentration. These results demonstrated that the efficient surface properties of ZnO NPs and ZnO/KC NCs enable the materials to yield enhanced antibacterial efficacies.

3.5. Antioxidant activity of ZnO NPs and ZnO/KC NCs

The body can be protected from the harmful effects of free radicals by the compounds name antioxidants that work through the process of scavenging free radicals. To check the antioxidant activity of synthesized ZnO NPs and ZnO/KC NCs, a DPPH (2, 2-diphenyl-1-picrylhydrazyl) scavenging assay was used at various concentrations of the developed catalysts i.e., 100, 200 and 300 μg/mL. Ascorbic acid (AA) was used as a standard in this process. The conclusive results in Fig. 8 display that as-synthesized ZnO NPs and ZnO/KC NCs have antioxidant activity less than the widely recognized ascorbic acid (standard), however, the values are still in the promising range compared to reported values in literature. The maximum impact of free radical scavenging was observed in ZnO/KC (70%) as compared to the AA (standard), while moderate activity was observed in ZnO NPs (52%) at 300 μg/mL.

4. Conclusion

In conclusion, we have successfully formed the ZnO NPs and ZnO/KC NCs and confirmed their morphology and structural behaviour from the SEM, XRD and FTIR. The nanoscale size of ZnO NPs and intercalated hydrophilic behaviour of KC enable the ZnO/KC NCs to effectively degrade the MR dye within 10 min. We established a relationship between various parameters and dye degradation that included catalyst amount, irradiation time, pH impact etc. Moreover, the ZnO/KC NCs also demonstrated superior performance after recovering from the various runs. Lastly, we have seen that the same system can be extended to antibacterial and antioxidant activities. About 21 and 24 mm of inhibition zone was found against *Citrobacter* and 22 and 23 mm of inhibition zone was observed against *Providencia* by ZnO NPs and ZnO/KC NCs, respectively at 100 μL of concentration. Similarly the maximum impact of free radical scavenging observed in ZnO/KC was 70%, while the activity displayed by ZnO NPs was 52% at 300 μg/mL. These outcomes suggested that the synthesized nanomaterials can be further modified and explored for photocatalytic and biological applications.

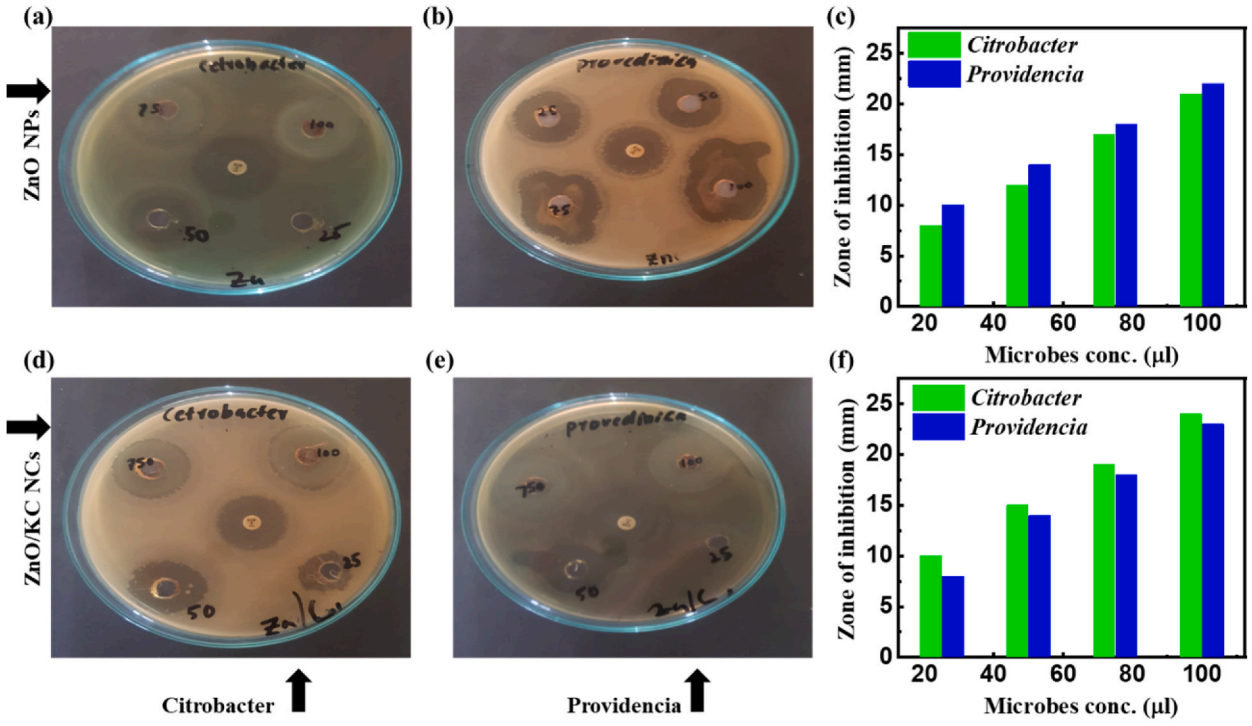

Fig. 7. Antibacterial activity analyses: **(a,b)** Digital images acquired from ZnO NPs against *Citrobacter* and *Providencia,* **(c)** graphical comparison against ZnO NPs. **(d,e)** Digital images acquired from ZnO/KC NCs against *Citrobacter* and *Providencia,* **(f)** graphical comparison against ZnO/KC NCs.

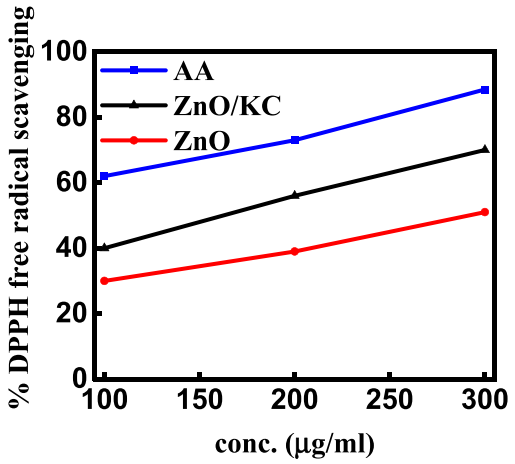

Fig. 8. Antioxidant assay: % DPPH free radical scavenging activity of ZnO NPs and ZnO/KC NCs.

Author contribution statement

Tamanna Gul: Performed the experiments.
Idrees Khan: Analyzed and interpreted the data; Wrote the paper.
Bashir Ahmad, Khalid Saeed: Conceived and designed the experiments.
Shujaat Ahmad: Performed the experiments; Analyzed and interpreted the data.
Ahad Amer Alsaiari, Mazen Almehmadi: Analyzed and interpreted the data.
Osama Abdulaziz, Abdulaziz Alsharif: Contributed reagents, materials, analysis tools or data.
Ibrahim Khan: Analyzed and interpreted the data; Contributed reagents, materials, analysis tools or data.

Data availability statement

No data was used for the research described in the article.

Funding

The researchers would like to acknowledges deanship of scientific research, Taif University and Brain Pool program under the Ministry of Science and ICT through the National Research Foundation of Korea (grant number NRF-2021H1D3A2A02044205) for funding of this work.

Declaration of competing interest

The authors declare that they have no known competing financial interests or personal relationships that could have appeared to influence the work reported in this paper.

Acknowledgements

The authors thank the Department of Chemistry, Bacha Khan University, Khyber Pakhtunkhwa, Pakistan for the required support in finalizing this manuscript.

References

[1] Z.Z. Gao, N. Qi, W.J. Chen, H. Zhao, Construction of hydroxyethyl cellulose/silica/graphitic carbon nitride solid foam for adsorption and photocatalytic degradation of dyes, Arab. J. Chem. 15 (2022), 104105, https://doi.org/10.1016/J.ARABJC.2022.104105.
[2] Z. Wang, M. Hu, Q. Wang, L. Li, Efficient and sustainable photocatalytic degradation of dye in wastewater with porous and recyclable wood foam@V2O5 photocatalysts, J. Clean. Prod. 332 (2022), 130054, https://doi.org/10.1016/J.JCLEPRO.2021.130054.
[3] K. Seku, S.S. Hussaini, M. Hussain, M.A. Siddiqui, N. Golla, D. Ravinder, B. Reddy G, Synthesis of Frankincense gum stabilized AgNPs by microwave irradiation and their catalytic, antioxidant, and antibacterial properties, Phys. E Low-Dimensional Syst. Nanostructures 140 (2022), 115169, https://doi.org/10.1016/J.PHYSE.2022.115169.
[4] K. Seku, G. Bhagavanth Reddy, S.S. Hussaini, B. Pejjai, M. Hussain, D.M. Reddy, M.A.K. Khazaleh, G. Mangatayaru, An efficient biosynthesis of palladium nanoparticles using Bael gum and evaluation of their catalytic and antibacterial activity, Int. J. Biol. Macromol. 209 (2022) 912–922, https://doi.org/10.1016/J.IJBIOMAC.2022.04.070.
[5] H. Shen, W. Zhang, C. Guo, J. Zhu, J. Cui, Z. Xue, P. Chen, Natural cotton cellulose-supported TiO2 quantum dots for the highly efficient photocatalytic degradation of dyes, Nanomaterials 12 (2022) 3130, https://doi.org/10.3390/NANO12183130/S1.

[6] Z. Liu, H. Tan, D. Liu, X. Liu, J. Xin, J. Xie, M. Zhao, L. Song, L. Dai, H. Liu, Z.H. Liu, H. Liu, H. Tan, J.P. Xin, D.B. Liu, L. Song, X.B. Liu, M.W. Zhao, J.F. Xie, L. M. Dai, Promotion of overall water splitting activity over a wide pH range by interfacial electrical effects of metallic NiCo-nitrides nanoparticle/NiCo2O4 nanoflake/graphite fibers, Adv. Sci. 6 (2019), 1801829, https://doi.org/10.1002/ADVS.201801829.

[7] R.R. Bhagavanth, R. Dadigala, R. Bandi, K. Seku, D. Koteswararao, G. Mangatayaru K, A.E. Shalan, Microwave-assisted preparation of a silver nanoparticles/N-doped carbon dots nanocomposite and its application for catalytic reduction of rhodamine B, methyl red and 4-nitrophenol dyes, RSC Adv. 11 (2021) 5139–5148, https://doi.org/10.1039/D0RA10679H.

[8] N. Nadeem, M. Zahid, Z.A. Rehan, M.A. Hanif, M. Yaseen, Improved photocatalytic degradation of dye using coal fly ash-based zinc ferrite (CFA/ZnFe2O4) composite, Int. J. Environ. Sci. Technol. 19 (2022) 3045–3060, https://doi.org/10.1007/S13762-021-03255-9/TABLES/2.

[9] M. Ashraf, N. Ullah, I. Khan, W. Tremel, S. Ahmad, M. Nawaz Tahir, Photoreforming of waste polymers for sustainable hydrogen fuel and chemicals feedstock: waste to energy, Chem. Rev. (2023), https://doi.org/10.1021/acs.chemrev.2c00602.

[10] I. Khan, J.H. Lee, J. Park, S. Wooh, Nano/micro-structural engineering of Nafion membranes for advanced electrochemical applications, J. Saudi Chem. Soc. 26 (2022), https://doi.org/10.1016/j.jscs.2022.101511.

[11] I. Khan, Strategies for improved electrochemical CO 2 reduction to value-added products by highly anticipated copper-based nanoarchitectures, Chem. Rec. 22 (2022), https://doi.org/10.1002/tcr.202100219 tcr.202100219.

[12] M. Mansha, T. Ahmad, N. Ullah, S. Akram Khan, M. Ashraf, S. Ali, B. Tan, I. Khan, Photocatalytic water-splitting by organic conjugated polymers: opportunities and challenges, Chem. Rec. 22 (2022), 202100336, https://doi.org/10.1002/TCR.202100336.

[13] M. Ashraf, I. Khan, N. Baig, A.H. Hendi, M.F. Ehsan, N. Sarfraz, A bifunctional 2D interlayered β-Cu 2 V 2 O 7/Zn 2 V 2 O 6 (CZVO) heterojunction for solar-driven nonsacrificial dye degradation and water oxidation, Energy Technol. 9 (2021), 2100034, https://doi.org/10.1002/ente.202100034.

[14] K. Xie, J. Fang, L. Li, J. Deng, F. Chen, Progress of graphite carbon nitride with different dimensions in the photocatalytic degradation of dyes: a review, J. Alloys Compd. 901 (2022), 163589, https://doi.org/10.1016/J.JALLCOM.2021.163589.

[15] S. Khan, A. Noor, I. Khan, M. Muhammad, M. Sadiq, N. Muhammad, Photocatalytic degradation of organic dyes contaminated aqueous solution using binary CdTiO2 and ternary NiCdTiO2 nanocomposites, Catalyst 13 (2023) 44, https://doi.org/10.3390/CATAL13010044.

[16] K. Vinothkumar, M. Shivanna Jyothi, C. Lavanya, M. Sakar, S. Valiyaveettil, R.G. Balakrishna, Strongly co-ordinated MOF-PSF matrix for selective adsorption, separation and photodegradation of dyes, Chem. Eng. J. 428 (2022), 132561, https://doi.org/10.1016/J.CEJ.2021.132561.

[17] M. Mondal, S. Banerjee, S. Mal, S. Das, S.K. Pradhan, Nanocomposites of GaBr3and BiBr3Nanocrystals on BiOBr for the photocatalytic degradation of dyes and tetracycline, ACS Appl. Nano Mater. 5 (2022) 15676–15691, https://doi.org/10.1021/ACSANM.2C03696/ASSET/IMAGES/LARGE/AN2C03696_0008 (JPEG).

[18] Y. Cui, C. Lin, M. Li, N. Zhu, J. Meng, J. Zhao, CuWO4/CuS heterojunction photocatalyst for the application of visible-light-driven photodegradation of dye pollution, J. Alloys Compd. 893 (2022), 162181, https://doi.org/10.1016/J.JALLCOM.2021.162181.

[19] K.P. Anjali, R. Raghunathan, G. Devi, S. Dutta, Photocatalytic degradation of methyl red using seaweed mediated zinc oxide nanoparticles, Biocatal. Agric. Biotechnol. 43 (2022), 102384, https://doi.org/10.1016/J.BCAB.2022.102384.

[20] C.M. Khor, M.M. Khan, A. Khan, M.Y. Khan, M.H. Harunsani, Zr, La-dual doped silver niobate for photocatalytic degradation of dyes under visible light irradiation, Heliyon 8 (2022), e10264, https://doi.org/10.1016/J.HELIYON.2022.E10264.

[21] I. Khan, M. Sadiq, I. Khan, K. Saeed, Manganese dioxide nanoparticles/activated carbon composite as efficient UV and visible-light photocatalyst, Environ. Sci. Pollut. Res. 26 (2019) 5140–5154, https://doi.org/10.1007/s11356-018-4055-y.

[22] T. Tatarchuk, N. Danyliuk, A. Shyichuk, W. Macyk, M. Naushad, Photocatalytic degradation of dyes using rutile TiO2 synthesized by reverse micelle and low temperature methods: real-time monitoring of the degradation kinetics, J. Mol. Liq. 342 (2021), 117407, https://doi.org/10.1016/J.MOLLIQ.2021.117407.

[23] M. Khatri, A. Gupta, K. Gyawali, A. Adhikari, A.R. Koirala, N. Parajuli, Photocatalytic degradation of dyes using synthesized δ-MnO2 nanostructures, Chem. Data Collect. 39 (2022), 100854, https://doi.org/10.1016/J.CDC.2022.100854.

[24] K. Alsamhary, N.M. Al-Enazi, E. Alhomaidi, S. Alwakeel, Spirulina platensis mediated biosynthesis of Cuo Nps and photocatalytic degradation of toxic azo dye Congo red and kinetic studies, Environ. Res. 207 (2022), 112172, https://doi.org/10.1016/J.ENVRES.2021.112172.

[25] M.F. Lanjwani, M.Y. Khuhawar, T.M.J. Khuhawar, A.H. Lanjwani, S.Q. Memon, W.A. Soomro, I.K. Rind, Photocatalytic degradation of eriochrome black T dye by ZnO nanoparticles using multivariate factorial, kinetics and isotherm models, J. Cluster Sci. (2022) 1–12, https://doi.org/10.1007/S10876-022-02293-8/FIGURES/8.

[26] P. Peerakiatkhajohn, T. Butburee, J.H. Sul, S. Thaweesak, J.H. Yun, Efficient and rapid photocatalytic degradation of methyl orange dye using Al/ZnO nanoparticles, Nanomaterials 11 (2021) 1059, https://doi.org/10.3390/NANO11041059.

[27] M.G. Batterjee, A. Nabi, M.R. Kamli, K.A. Alzahrani, E.Y. Danish, M.A. Malik, Green hydrothermal synthesis of zinc oxide nanoparticles for UV-Light-Induced photocatalytic degradation of ciprofloxacin antibiotic in an aqueous environment, Catalyst 12 (2022) 1347, https://doi.org/10.3390/CATAL12111347.

[28] A. Serrano-Lázaro, F.A. Verdín-Betancourt, V.K. Jayaraman, A. Hernández-Gordillo, M. de L. López-González, A. Sierra-Santoyo, G. Santana, M. Bizarro, Tracing the degradation pathway of temephos pesticide achieved with photocatalytic ZnO nanostructured films, Environ. Sci. Nano. 9 (2022) 3538–3550, https://doi.org/10.1039/D2EN00384H.

[29] H. Subramanian, M. Krishnan, A. Mahalingam, Photocatalytic dye degradation and photoexcited anti-microbial activities of green zinc oxide nanoparticles synthesized via Sargassum muticum extracts, RSC Adv. 12 (2022) 985–997, https://doi.org/10.1039/D1RA08196A.

[30] H. Agarwal Prerna, D. Goyal, Photocatalytic degradation of textile dyes using phycosynthesised ZnO nanoparticles, Inorg. Chem. Commun. 142 (2022), 109676, https://doi.org/10.1016/J.INOCHE.2022.109676.

[31] D.T.C. Nguyen, H.T.N. Le, T.T. Nguyen, T.T.T. Nguyen, L.G. Bach, T.D. Nguyen, T. Van Tran, Multifunctional ZnO nanoparticles bio-fabricated from Canna indica L. flowers for seed germination, adsorption, and photocatalytic degradation of organic dyes, J. Hazard Mater. 420 (2021), 126586, https://doi.org/10.1016/J.JHAZMAT.2021.126586.

[32] K. Saeed, I. Khan, M. Ahad, T. Shah, M. Sadiq, A. Zada, N. Zada, Preparation of ZnO/Nylon 6/6 nanocomposites, their characterization and application in dye decolorization, Appl. Water Sci. 11 (2021) 105, https://doi.org/10.1007/s13201-021-01442-0.

[33] K. Saeed, I. Khan, Z. Ahmad, B. Khan, Preparation, analyses and application of cobalt–manganese oxides/nylon 6,6 nanocomposites, Polym. Bull. 75 (2018), https://doi.org/10.1007/s00289-018-2292-3.

[34] I. Khan, N. Zada, I. Khan, M. Sadiq, K. Saeed, Enhancement of photocatalytic potential and recoverability of Fe3O4 nanoparticles by decorating over monoclinic zirconia, J. Environ. Heal. Sci. Eng. 18 (2020) 1473–1489, https://doi.org/10.1007/s40201-020-00563-z.

[35] A.H. Jawad, A.S. Abdulhameed, E. Kashi, Z.M. Yaseen, Z.A. Alothman, M.R. Khan, Cross-linked chitosan-glyoxal/kaolin clay composite: parametric optimization for color removal and COD reduction of remazol brilliant blue R dye, J. Polym. Environ. 30 (2022) 164–178, https://doi.org/10.1007/S10924-021-02188-1/FIGURES/8.

[36] M. Ashrul Asbollah, M.S.M. Sahid, K.M. Padmosoedarso, A.H. Mahadi, E. Kusrini, J. Hobley, A. Usman, Individual and competitive adsorption of negatively charged acid blue 25 and acid red 1 onto raw Indonesian kaolin clay, Arabian J. Sci. Eng. 47 (2022) 6617–6630, https://doi.org/10.1007/S13369-021-06498-3/FIGURES/10.

[37] M. Almatari, Y. Koraim, I.H. Saleh, M.I. Sayyed, M. Uddin Khandaker, M. Elsafi, Investigation of the photon shielding capability of kaolin clay added with micro and nanoparticles of Bi2O3, Radiat. Phys. Chem. 200 (2022), 110191, https://doi.org/10.1016/J.RADPHYSCHEM.2022.110191.

[38] S. Mustapha, J.O. Tijani, M.M. Ndamitso, S.A. Abdulkareem, D.T. Shuaib, A.K. Mohammed, A. Sumaila, The role of kaolin and kaolin/ZnO nanoadsorbents in adsorption studies for tannery wastewater treatment, Sci. Rep. 10 (2020) 1–22, https://doi.org/10.1038/s41598-020-69808-z.

[39] H. Bel Hadjltaief, M. Ben Zina, M.E. Galvez, P. Da Costa, Photocatalytic degradation of methyl green dye in aqueous solution over natural clay-supported ZnO–TiO2 catalysts, J. Photochem. Photobiol. Chem. 315 (2016) 25–33, https://doi.org/10.1016/J.JPHOTOCHEM.2015.09.008.

[40] M.K. Uddin, A review on the adsorption of heavy metals by clay minerals, with special focus on the past decade, Chem. Eng. J. 308 (2017) 438–462, https://doi.org/10.1016/J.CEJ.2016.09.029.

[41] A.T. Le, S.Y. Pung, S. Sreekantan, A. Matsuda, D.P. Huynh, Mechanisms of removal of heavy metal ions by ZnO particles, Heliyon 5 (2019), e01440, https://doi.org/10.1016/J.HELIYON.2019.E01440.

[42] S. Mustapha, M.M. Ndamitso, A.S. Abdulkareem, J.O. Tijani, D.T. Shuaib, A.O. Ajala, A.K. Mohammed, Application of TiO2 and ZnO nanoparticles immobilized on clay in wastewater treatment: a review, Appl. Water Sci. 101 (2020) 1–36, https://doi.org/10.1007/S13201-019-1138-Y.
[43] S. Alamdari, M.S. Ghamsari, C. Lee, W. Han, H.H. Park, M.J. Tafreshi, H. Afarideh, M.H.M. Ara, Preparation and characterization of zinc oxide nanoparticles using leaf extract of Sambucus ebulus, Appl. Sci. 10 (2020) 3620, https://doi.org/10.3390/APP10103620.
[44] K. Muralishwara, Y.N. Sudhakar, U.A. Kini, S. Sharma, B.M. Gurumurthy, Moisture absorption and spectroscopic studies of epoxy clay nanocomposite, Polym. Bull. 79 (2022) 5587–5611, https://doi.org/10.1007/S00289-022-04200-7/FIGURES/22.
[45] K. Mamulová Kutláková, J. Tokarský, P. Peikertová, Functional and eco-friendly nanocomposite kaolinite/ZnO with high photocatalytic activity, Appl. Catal. B Environ. 162 (2015) 392–400, https://doi.org/10.1016/J.APCATB.2014.07.018.
[46] I. Khan, Pluronic-123 assisted synthesis of cobalt vanadate microparticles (μ-CoV MPs) for durable electrochemical oxygen evolution reaction in seawater and connate water, Catalysts 13 (2023) 636, https://doi.org/10.3390/CATAL13030636.
[47] I. Khan, S. Ali, M. Mansha, A. Qurashi, Sonochemical assisted hydrothermal synthesis of pseudo-flower shaped Bismuth vanadate (BiVO4) and their solar-driven water splitting application, Ultrason. Sonochem. 36 (2017) 386–392, https://doi.org/10.1016/J.ULTSONCH.2016.12.014.
[48] H.S. Wai, C. Li, Fabrication of well-aligned ZnO nanorods with different reaction times by chemical bath deposition method applying for photocatalysis application, Mol 28 (2023) 397, https://doi.org/10.3390/MOLECULES28010397.
[49] F.F. Alharbi, S. Manzoor, T. Munawar, M.U. Nisa, A.G. Abid, F. Iqbal, S. Aman, M.F. Ehsan, M. Najam-Ul-Haq, M.N. Ashiq, Sunlight activated S-scheme ZnO-CoTe binary photocatalyst for effective degradation of dye pollutants from wastewater, Surface. Interfac. 31 (2022), 101991, https://doi.org/10.1016/J.SURFIN.2022.101991.
[50] M. Afsharpour, S. Amoee, Porous biomorphic silica@ZnO nanohybrids as the effective photocatalysts under visible light, Environ. Sci. Pollut. Res. 29 (2022) 49784–49795, https://doi.org/10.1007/S11356-022-19377-7/FIGURES/10.
[51] Y.C. Goswami, J.B. Kaundal, S. Begzaad, R.K. Tiwari, Photocatalytic degradation of Methyl Red dye using highly efficient ZnO/CdS hierarchical heterostructures under white LED, J. Iran. Chem. Soc. (2023) 1–17, https://doi.org/10.1007/S13738-023-02789-8/FIGURES/13.
[52] F. Anjum, A.M. Asiri, M.A. Khan, M.I. Khan, S.B. Khan, K. Akhtar, E.M. Bakhsh, K.A. Alamry, S.Y. Alfifi, S. Chakraborty, Photo-degradation, thermodynamic and kinetic study of carcinogenic dyes via zinc oxide/graphene oxide nanocomposites, J. Mater. Res. Technol. 15 (2021) 3171–3191, https://doi.org/10.1016/J.JMRT.2021.09.086.
[53] N. Khan, T. Gul, I. Khan, E.A. Alabbad, S. Ali, K. Saeed, I. Khan, Scavenging of organic pollutant and fuel generation through cost-effective and abundantly accessible rust: a theoretical support with DFT simulations, Materials 16 (2022) 142, https://doi.org/10.3390/ma16010142.
[54] S. Zhou, J. Bai, K. Huang, X. Ye, Y. Peng, M. Lei, Consideration of photoactivity of TiO2 pigments via the photodegration of methyl orange under UV irradiation, Materials 15 (2022) 6044, https://doi.org/10.3390/MA15176044/S1.
[55] I. Khan, K. Saeed, N. Ali, I. Khan, B. Zhang, M. Sadiq, Heterogeneous photodegradation of industrial dyes: an insight to different mechanisms and rate affecting parameters, J. Environ. Chem. Eng. 8 (2020), https://doi.org/10.1016/j.jece.2020.104364.
[56] S. Ahmad, M. Almehmadi, H.T. Janjuhah, G. Kontakiotis, O. Abdulaziz, K. Saeed, H. Ahmad, M. Allahyani, A. Aljuaid, A.A. Alsaiari, J. Muhammad, I. Khan, The effect of mineral ions present in tap water on photodegradation of organic pollutants: future perspectives, Water 15 (2023) 175, https://doi.org/10.3390/W15010175.
[57] N.K. Singh, S. Saha, A. Pal, Methyl red degradation under UV illumination and catalytic action of commercial ZnO: a parametric study, Desalination Water Treat. 56 (2015) 1066–1076, https://doi.org/10.1080/19443994.2014.942380.
[58] N.K. Singh, S. Saha, A. Pal, Solar light-induced photocatalytic degradation of methyl red in an aqueous suspension of commercial ZnO: a green approach, Desalination Water Treat. 53 (2015) 501–514, https://doi.org/10.1080/19443994.2013.838520.
[59] X. Chen, Z. Wu, D. Liu, Z. Gao, Preparation of ZnO photocatalyst for the efficient and rapid photocatalytic degradation of azo dyes, Nanoscale Res. Lett. 12 (2017) 1–10, https://doi.org/10.1186/S11671-017-1904-4/FIGURES/12.
[60] W. Ben Mbarek, L. Escoda, J. Saurina, E. Pineda, F.M. Alminderej, M. Khitouni, J.J. Suñol, Nanomaterials as a sustainable choice for treating wastewater: a review, Mater 15 (2022) 8576, https://doi.org/10.3390/MA15238576.
[61] J. An, N.T.H. Nhung, Y. Ding, H. Chen, C. He, X. Wang, T. Fujita, Chestnut shell-activated carbon mixed with pyrolytic snail shells for methylene blue adsorption, Mater 15 (2022) 8227, https://doi.org/10.3390/MA15228227.
[62] T. Gul, I. Khan, S. Ali, M. Sadiq, K. Saeed, Synthesis and characterization of Mn-Pt/AC nanoparticles and their photocatalytic and antibacterial applications, J. Dispersion Sci. Technol. 43 (2022) 612–619, https://doi.org/10.1080/01932691.2020.1844732.
[63] S. Sudhasree, A. Shakila Banu, P. Brindha, G.A. Kurian, Synthesis of nickel nanoparticles by chemical and green route and their comparison in respect to biological effect and toxicity, Toxicol. Environ. Chem. 96 (2014) 743–754, https://doi.org/10.1080/02772248.2014.923148.